IR and Raman spectra of liquid water: Theory and interpretation

Cite as: J. Chem. Phys. **128**, 224511 (2008); https://doi.org/10.1063/1.2925258
Submitted: 30 January 2008 . Accepted: 18 April 2008 . Published Online: 12 June 2008

B. M. Auer, and J. L. Skinner

IR and Raman spectra of liquid water: Theory and interpretation

B. M. Auer and J. L. Skinner[a)]
Theoretical Chemistry Institute and Department of Chemistry, University of Wisconsin, Madison, Wisconsin 53706, USA

(Received 30 January 2008; accepted 18 April 2008; published online 12 June 2008)

IR and Raman (parallel- and perpendicular-polarized) spectra in the OH stretch region for liquid water were measured some years ago, but their interpretation is still controversial. In part, this is because theoretical calculation of such spectra for a neat liquid presents a formidable challenge due to the coupling between vibrational chromophores and the effects of motional narrowing. Recently we proposed an electronic structure/molecular dynamics method for calculating spectra of dilute HOD in liquid D_2O, which relied on *ab initio* calculations on clusters to provide a map from nuclear coordinates of the molecules in the liquid to OH stretch frequencies, transition dipoles, and polarizabilities. Here we extend this approach to the calculation of couplings between chromophores. From the trajectories of the fluctuating local-mode frequencies, transition moments, and couplings, we use our recently developed time-averaging approximation to calculate the line shapes. Our results are in good agreement with experiment for the IR and Raman line shapes, and capture the significant differences among them. Our analysis shows that while the coupling between chromophores is relatively modest, it nevertheless produces delocalization of the vibrational eigenstates over up to 12 chromophores, which has a profound effect on the spectroscopy. In particular, our results demonstrate that the peak in the parallel-polarized Raman spectrum at about 3250 wavenumbers is collective in nature. © *2008 American Institute of Physics*. [DOI: 10.1063/1.2925258]

I. INTRODUCTION

Understanding the structure and dynamics of liquid water remains an important and challenging research problem. Infrared (IR) and Raman spectroscopies in the OH stretch region have played a major role in this regard, since OH stretch frequencies are very sensitive to molecular environments. The IR spectrum of water at room temperature and 1 atm pressure[1–3] is peaked at about 3400 cm^{-1}, has a weak shoulder at about 3250 cm^{-1}, and a full width at half maximum (FWHM) of about 375 cm^{-1}. Raman spectra are quite different:[4–11] the parallel-polarized (VV) spectrum is bimodal, with strong peaks at about 3400 and 3250 cm^{-1}, and a FWHM of about 425 cm^{-1}, while the perpendicular-polarized (VH) spectrum peaks at about 3460 cm^{-1}, is quite asymmetric and has a FWHM of about 300 cm^{-1}. Note that the gas-phase water molecule has symmetric and antisymmetric stretch fundamentals (both of which are IR and Raman active) at 3657 and 3756 cm^{-1}, respectively, and so the liquid-state spectra are significantly redshifted from these values, and furthermore, the breadths of the liquid-state spectra are substantially larger than this gas-phase splitting.

A common interpretation of these spectra comes from fitting them to several Gaussians, centered at different positions, each with a different width. One then often attributes each Gaussian to a particular molecular environment and/or normal mode. Thus, for example, both IR and Raman spectra of liquid water have been deconstructed in this way, and the various Gaussians are attributed to molecules in different classes of hydrogen-bonded environments, sometimes with further designations of symmetric or antisymmetric stretch normal modes.[2,4–9,12] The results from such a procedure, together with the observation of approximate isospestic points in temperature-dependent spectra, have been interpreted as supporting mixture models of water.[2,4–9,12] However, Geissler has recently shown that isospestic points can occur quite generally, and therefore do not necessarily imply multiple species.[13]

Others have argued that the complications of intramolecular and intermolecular vibrational couplings make simple interpretations of these spectra difficult.[10,11,14–17] In fact, many believe that the lower-frequency peak in the VV Raman spectrum arises from a collective mode.[10,11,15,16] By performing isotopic replacement studies, in particular, focusing on the case of dilute HOD in D_2O,[14,17–19] the effects of both intramolecular and intermolecular vibrational couplings of the OH stretch to other vibrational modes are mitigated. To the extent that the structure and dynamics of D_2O are similar to those of normal water, then, the HOD molecule functions as an excellent localized probe of liquid water. In any case, the IR spectrum in the OH stretch region for this system shows a slightly asymmetric but monomodal line shape, peaked at about 3400 cm^{-1} with a FWHM of about 250 cm^{-1}. In this case, the VV and VH Raman spectra are quite similar to each other,[4,5] peaking at about 3430 cm^{-1}, with a quite prominent shoulder at about 3600 cm^{-1}, and a FWHM of about 300 cm^{-1}.

The monomodal shapes of the HOD/D_2O IR and Raman spectra and their simple temperature dependencies might seem to favor continuum (over mixture) models of water.[14,17]

[a)]Electronic mail: skinner@chem.wisc.edu.

To quote from the 1966 paper by Falk and Ford: "The infrared spectra of HDO thus fully support the continuum models and are incompatible with the existence in water of any discrete molecular species differing in the extent of hydrogen bonding." Indeed, from the viewpoint of modern liquid-state statistical mechanics the continuum picture seems more natural. As an attempt to find some common ground between the extremes of mixture and continuum models, we note that with a suitable hydrogen bond definition,[20] one can always classify any molecule according to its instantaneous hydrogen-bonding environment.[21–23] If the frequency distributions of these classes are relatively narrow and nonoverlapping this would support a mixture model,[12] but if the frequency distributions are relatively broad and overlapping this would support a continuum model. Our latest theoretical work in this regard[23] indicates that many of the frequency distributions are broad and overlapping, thus supporting the continuum picture, although the frequency distributions corresponding to HOD molecules lacking a hydrogen bond to the H are relatively narrow.

All of these vibrational spectra have generated significant theoretical interest. Focusing first on the relatively simpler case of HOD/D_2O, most of the theoretical calculations have been of a mixed quantum/classical nature. With the exception of the OH stretch all the molecules are treated as rigid (nonvibrating). The thinking here is that since ($\hbar$ times) the frequencies of bend and OD stretch modes of all molecules are significantly higher than kT, and since none of these modes is thermally or otherwise excited (all of these modes exist in their ground quantum states), it is perhaps better to keep them rigid than to allow them to vibrate classically. The translations and rotations of all molecules are treated classically with molecular dynamics (MD) simulation. One should note here that this classical treatment of the relatively high frequency librational motions is highly questionable. For a given molecular configuration generated by the simulation the OH stretch is then typically treated quantum mechanically. The solvent-induced frequency shift from a reference gas-phase value can be calculated using the empirical simulation potential and certain diagonal matrix elements,[21,22,24–26] or by solving the one-dimensional (1D) quantum mechanics of the OH stretch adiabatically and determining the fundamental frequency.[27–31] Alternatively one can use *ab initio* electronic structure (ES) calculations to determine the appropriate adiabatic potential.[32] Two groups have married this approach to MD simulations with the use of "maps" from nuclear configuration of the solute/solvent system to OH stretch frequency.[33–36] Any of these approaches allow one to calculate a frequency trajectory from the simulation, and hence an approximation to IR and Raman line shapes that includes the effects of motional narrowing.[24,37–39] In addition, non-Condon effects (the magnitude of the OH transition dipole depends on the molecular environment of the HOD molecule) are important for water, and these can be taken into account in a similar manner.[23,40–42] Our latest work along these lines[23] gives IR and Raman spectra in reasonable agreement with experiment.

Theoretical work on vibrational spectroscopy in H_2O is more limited, as this system is substantially more complicated (as alluded to above). Rice and co-workers emphasized the role of intramolecular and intermolecular vibrational couplings, diagonalizing the vibrational Hamiltonian for configurations (albeit time averaged for 66 fs) generated from a MD simulation.[15,16] A similar approach has been implemented more recently by Bouř.[43] A related approach was also presented by Reimers and Watts.[44] An alternative and much easier approach for this problem is to treat classically all degrees of freedom (including the OH stretches), and hence calculate spectra from the classical dipole time-correlation function from a MD simulation of flexible molecules,[45–49] or from a Car–Parrinello simulation.[50] These classical approaches might be suspect because the OH stretch is very anharmonic and has a frequency high compared to kT; thus a classical simulation does not access the part of the anharmonic potential that is relevant for vibrational spectroscopy.

Very recently mixed quantum/classical approaches that include dynamical effects have been presented by Buch *et al.*[51,52] and by Torii.[53] In the former calculation the configurations were generated by MD simulation; the local-mode anharmonic OH stretch frequencies were determined by a map of the nature described above (but in this case parametrized from spectroscopic experiments on clusters[54] rather than from *ab initio* calculations[33–36]), and were then time averaged for 1 ps to approximate the effects of motional narrowing. Intermolecular couplings were taken to arise from interacting transition dipoles for the OH stretch chromophores. Similar calculations by Torii[53] exactly treat the effects of motional narrowing, but in doing so require extensive numerical computations.

The calculation of vibrational line shapes and other spectroscopic observables for the case of many coupled chromophores is a difficult theoretical problem, and has captured the attention of a number of theorists in recent years.[24,51–65] If dynamics are unimportant (the inhomogeneous limit), the problem simplifies considerably. If the dynamics are important, but the problem can be treated adiabatically, the problem is still relatively simple. However, for several problems of experimental and theoretical interest (such as water, and coupled amide stretches in peptides and proteins), neither the inhomogeneous nor adiabatic approximations are appropriate. Nonetheless, within the mixed quantum/classical approach, the problem can still be formulated exactly, thus fully including nonadiabatic effects and motional narrowing. For a few coupled chromophores this approach can be implemented relatively easily,[55,58,65,66] but for many interacting chromophores such an exact calculation represents a daunting task,[53] and it can be difficult to obtain good statistics.

Given the above, and especially considering the case of nonlinear observables, it would be useful to develop less time-consuming (but necessarily more approximate) approaches to this problem. In a recent paper[55] we proposed a strategy to this end. It is based on the idea that motional narrowing can be thought of as arising from a distribution of time-averaged frequencies. For an isolated chromophore, motional narrowing occurs when the dynamics of the frequency fluctuations are sufficiently fast that they "self-average" (to some extent). The idea then is that one can

average a frequency trajectory over time windows of duration T, to obtain a distribution of these time-averaged frequencies, which is of course narrower than the actual distribution of frequencies. This idea has antecedents in earlier papers by Rice,[15] Hermansson,[38] Buch,[51] but was only recently formalized.[55] From an analysis of the Kubo model,[37] we showed[55] that the appropriate averaging time is approximately given by the very simple formula $T \simeq 5/\Gamma$, where Γ is the FWHM of the actual line shape. Of course for an isolated chromophore, there is no problem obtaining the actual line shape, and consequently no need to use the time-averaging approximation (TAA). However, for many interacting chromophores, the proposed strategy is to calculate first the line shape for noninteracting chromophores, identify the appropriate averaging time T, and then apply the TAA to the coupled system. We have tested the TAA on simple models with two coupled chromophores (the two OH stretch local modes in water) by comparing to exact calculations.[55] We expect that the TAA will work well for many coupled chromophores as long as the dynamics are not too fast, and the coupling between chromophores is not too large, as in the case of water discussed herein.

In this paper we present calculations for liquid H_2O that are similar in spirit but different in detail from those of Buch[51,52] and Torii.[53] The MD simulations are of the SPC/E model.[67] Local-mode anharmonic frequencies are generated from our most recent map developed for the HOD/D_2O system,[23] as are our transition dipoles. The relatively small intramolecular coupling fluctuates with molecular environment, and is determined herein by a separate map parametrized from *ab initio* calculations on clusters. The form of the intermolecular couplings is transition dipole, which is tested and parametrized from additional *ab initio* calculations. The effects of motional narrowing are approximately taken into account with the TAA.[55] Our results are in reasonably good agreement with experimental Raman (VV and VH) and IR spectra. Our analysis of the instantaneous vibrational eigenstates, which extend over up to 12 OH stretch chromophores, shows that attempts to interpret spectra with concepts involving the molecular environments of single water molecules are misguided, and that, for example, the origin of the VV Raman peak at about 3250 cm^{-1} is indeed collective in nature.

II. MIXED QUANTUM/CLASSICAL AND TIME-AVERAGING APPROXIMATION APPROACHES

Both IR and Raman line shapes can be written in terms of quantum time-correlation functions. In the IR case, if the electric field of the excitation light is polarized in the $\hat{\epsilon}$ direction, the linear absorption line shape is[68]

$$I(\omega) \sim \mathrm{Re} \int_0^\infty dt e^{-i\omega t} \langle \hat{\epsilon} \cdot \vec{\mu}(0) \vec{\mu}(t) \cdot \hat{\epsilon} \rangle, \tag{1}$$

where $\vec{\mu}(t)$ is the Heisenberg expression for the dipole operator of the system at time t, and the brackets indicate a quantum equilibrium statistical mechanical average. Taking $\hat{\epsilon}$ to be along one of the laboratory-fixed X, Y, or Z axes, the line shape can then be calculated from considering the time-correlation function of the component of the dipole, μ_p, where p denotes one of these axes.

In a typical Raman experiment the incident beam is polarized in a particular direction, call it $\hat{\epsilon}_0$, and the scattered beam is polarized in the $\hat{\epsilon}_s$ direction. Analogous to the IR line shape, the Raman line shape is the Fourier transform of the quantum polarizability time-correlation function:[68]

$$I(\omega) \sim \mathrm{Re} \int_0^\infty dt e^{-i\omega t} \langle \hat{\epsilon}_0 \cdot \underline{\alpha}(0) \cdot \hat{\epsilon}_s \hat{\epsilon}_0 \cdot \underline{\alpha}(t) \cdot \hat{\epsilon}_s \rangle, \tag{2}$$

where $\underline{\alpha}$ is the polarizability tensor operator for the system. If the scattered light has the same polarization as the incident light, this is referred to as the VV or parallel-polarized line shape. On the other hand, if the scattered light has a polarization perpendicular to the incident light this is referred to as the VH or perpendicular-polarized line shape. Thus the VV and VH line shapes can be determined by calculating the time-correlation functions of the appropriate tensor elements α_{pq}, where $p=q$ for the VV line shape, $p \neq q$ for the VH line shape, and as above p and q denote the X, Y, or Z axes in the laboratory frame.

To calculate these spectra, we will consider a mixed quantum/classical approach. The rotations and translations of the rigid water molecules will be treated by classical mechanics, with a MD simulation. The OH stretches will be treated quantum mechanically. For the purposes of this paper we will ignore the bends, thereby assuming that the 2:1 Fermi resonance (the stretch frequency is roughly twice that of the bend) does not appreciably affect these spectra. Therefore, we write the vibrational Hamiltonian for the liquid in the basis of single excitations of each OH chromophore. Thus at time t the (anharmonic fundamental) vibrational frequency of chromophore i is denoted $\omega_i(t)$, and the coupling (in frequency units) between chromophores i and j is denoted $\omega_{ij}(t)$. As indicated, these frequencies are time dependent since they depend on the configurations of the classical variables. In the next section, we will describe our model for the approximate calculation of these frequencies.

The dipole operator can be written as a sum of operators for each chromophore. Of interest in this mixed quantum/classical approach is the (laboratory-fixed) component p at time t of the transition dipole for chromophore i, which we will call $m_{ip}(t)$. Note that this changes in time as the molecule that contains chromophore i rotates, and hence the projection of its (molecule-fixed) unit vector on the laboratory axis fluctuates. In addition, the magnitude of the transition dipole itself depends on the classical variables (what we and other have been calling non-Condon effects). In a similar manner the polarizability tensor can be written as a sum of operators for each chromophore, and we will call $a_{ipq}(t)$, the pq component at time t of the transition polarizability for chromophore i. In the next section, we will describe our model for calculating these transition dipoles and polarizabilities.

Within this mixed quantum/classical approach the IR line shape can be written as[55]

$$I(\omega) \sim \mathrm{Re} \int_0^\infty dt e^{-i\omega t} \sum_{ij} \langle m_{ip}(0) F_{ij}(t) m_{jp}(t) \rangle e^{-t/2T_1}, \quad (3)$$

where $F_{ij}(t)$ are the elements of the matrix $F(t)$, which satisfies the equation

$$\dot{F}(t) = iF(t)\kappa(t), \quad (4)$$

subject to the initial condition that $F_{ij}(0) = \delta_{ij}$, and with

$$\kappa_{ij}(t) = \omega_i(t)\delta_{ij} + \omega_{ij}(t)(1 - \delta_{ij}). \quad (5)$$

Thus $\kappa(t)$ is a matrix whose diagonal elements are the fluctuating transition frequencies, $\omega_i(t)$, and whose off-diagonal elements are the fluctuating couplings $\omega_{ij}(t)$. The angular brackets now denote a classical equilibrium statistical mechanical average. Within this approach the effects of the lifetime of an OH stretch excitation in water, T_1, must be included phenomenologically, as shown; the value for T_1 will be taken from experiment.

The formulas for the Raman line shapes are similarly

$$I_{\mathrm{VV}}(\omega) \sim \mathrm{Re} \int_0^\infty dt e^{-i\omega t} \sum_{ij} \langle a_{ipp}(0) F_{ij}(t) a_{jpp}(t) \rangle e^{-t/2T_1}, \quad (6)$$

and

$$I_{\mathrm{VH}}(\omega) \sim \mathrm{Re} \int_0^\infty dt e^{-i\omega t} \sum_{ij} \langle a_{ipq}(0) F_{ij}(t) a_{jpq}(t) \rangle e^{-t/2T_1}, \quad (7)$$

where $p \neq q$.

It is computationally demanding to solve repeatedly the matrix differential equation in Eq. (4) for a large number of coupled chromophores. To this end several approximate results have been derived for line shapes for a system of coupled chromophores. We will focus on one of these, the so-called TAA.[55] The basic idea behind the TAA is that for an isolated chromophore one can approximate the effects of motional narrowing by considering a distribution of frequencies averaged over an appropriate time window. For the case of coupled chromophores the approximation is to average the matrix $\kappa(t)$. Thus in the TAA we replace $\kappa(t)$ in Eq. (4) with

$$\kappa_T = \frac{1}{T} \int_0^T dt' \kappa(t'), \quad (8)$$

which depends parametrically on the averaging time T, and in the case of the IR line shape we replace $m_{jp}(t)$ by $m_{jp}(T)$. For any one realization of the trajectory $\kappa(t)$, κ_T is diagonalized by the orthogonal transformation $N^T \kappa_T N$, and then the line shape can be written approximately as[55]

$$I(\omega) \sim \sum_k \langle d_k(0) d_k(T) L(\omega - \gamma_k) \rangle, \quad (9)$$

where

$$d_k(t) = \sum_i m_{ip}(t) N_{ik}, \quad (10)$$

and γ_k are the eigenvalues of κ_T. The delta function in our original work[55] has now been replaced by the Lorentzian

$$L(\omega) = \frac{1/2\pi T_1}{\omega^2 + (1/2T_1)^2} \quad (11)$$

to take into account lifetime broadening. Expressions for the Raman line shapes are identical, except $m_{ip}(t)$ is replaced by $a_{ipp}(t)$ or $a_{ipq}(t)$. The ensemble average in Eq. (9) is implemented as a time average over different starting points in the trajectory.

In our derivation of the TAA we suggested an algorithm to determine the averaging time T. Consider first the line shape for an uncoupled chromophore, without non-Condon effects, and rotational and lifetime broadening. We showed that to a good approximation the TAA result reproduces this line shape if the averaging time is given by $T \simeq 5/\Gamma$, where Γ is the FWHM of the line shape. Now for the coupled problem, including non-Condon effects and rotational and lifetime broadening, we simply choose the same averaging time.

III. DETERMINATION OF THE FLUCTUATING FREQUENCIES, COUPLINGS, AND TRANSITION DIPOLES AND POLARIZABILITIES

In order to calculate IR and Raman line shapes for liquid H_2O, we need to be able to relate the OH stretch frequencies ω_i, the couplings ω_{ij} between the local modes, the components of the transition dipoles m_{ip}, and the components of the transition polarizability tensors a_{ipq}, to the instantaneous environments of the OH stretches of interest. Thus in this section we provide prescriptions for obtaining the trajectories of the required fluctuating quantities from a MD simulation.

A. Fluctuating transition frequencies

In the ES/MD approach originally developed by Corcelli *et al.*[33] and most recently implemented by Auer *et al.*[23] random clusters of a solute molecule and the surrounding solvent molecules are extracted from a MD simulation. In the present case both the solvent and solute are H_2O. We generate 999 clusters by first selecting a H in our simulation of SPC/E water[67] at random every 500 fs to define the bond of interest. Any molecule having its oxygen within 4 Å of this hydrogen is included in the cluster, which results in an average cluster size of 9.25 waters. Finally, any other molecules within 7.831 Å have their positions recorded, as these nuclei will be included as point charges (using the SPC/E values) in the subsequent ES calculations. This set of clusters will be referred to as hydrogen centered. All ES calculations reported herein are performed at the B3LYP/6-311++G** level using the GAUSSIAN 03 software package.[69]

Next we calculate the local-mode OH stretching fundamental frequency for the bond of interest in each cluster. This is done by keeping all nuclei fixed except those on the molecule containing the bond of interest, and the relevant OH stretching coordinate is allowed to vary (keeping the center of mass and orientation of the molecule fixed), mapping out a 1D Born–Oppenheimer potential energy surface. Then we find the two lowest eigenvalues using a discrete variable representation (DVR).[70] We treat the H_2O as a pseudodiatomic, with a reduced mass of 0.951 44 amu. For the gas-phase molecule this procedure yields a local-mode

TABLE I. Empirical relationships for the transition frequency, dipole derivative, intramolecular coupling, and matrix elements. The electric field, E_i, at the H and in the direction of the OH bond, is in a.u. as are the matrix elements and intramolecular coupling k_{ij}^a. The correlation coefficient, R, and rms deviation of each fit are also listed.

Empirical relationship	R	rms deviation
$\omega_i=(3762-5060E_i-86225E_i^2)$ cm^{-1}	0.90	70.1 cm^{-1}
$x_i=0.1934-1.75\times10^{-5}(\omega_i/\text{cm}^{-1})$	1.00	1.1×10^{-4}
$\mu_i'/\mu_g'=0.7112+75.59E_i$	0.92	0.41
$p_i=1.611+5.893\times10^{-4}(\omega_i/\text{cm}^{-1})$	1.00	2.8×10^{-3}
$k_{ij}^a=-0.008149+0.1087(E_i+E_j)$	0.93	1.0×10^{-3}

anharmonic frequency of 3723 cm^{-1}. The corresponding experimental local-mode OH stretch fundamental in H_2O is of course unknown, but within the confines of the OH-stretch-only model, it can be estimated to be halfway between the symmetric and antisymmetric stretch frequencies, which gives 3706.5 cm^{-1}. The comparison of the calculated and experimental numbers suggests that our local-mode frequencies should all be multiplied by a scale factor of 0.9956. These scaled *ab initio* frequencies for each cluster are then fitted to a quadratic function of the component of the electric field along the OH bond, at the hydrogen, and the electric field is due to the (SPC/E) point charges on all molecules (except the tagged one) within the cutoff of 7.831 Å. It turns out that this map, giving the local-mode frequency for a given electric field, is nearly identical to that determined earlier for the OH stretch of HOD,[23] and so for simplicity we will use the previous formula, which is given in Table I. Calculated frequencies for a random subset of the clusters, together with the electric field fit, are shown in Fig. 1. The rms deviation of the *ab initio* frequencies from the fit is a not insubstantial 70 cm^{-1}. On the other hand, as shown in Fig. 2 of Ref. 23, the distribution of frequencies obtained from the MD simulation and the map is in good agreement with the actual distribution of *ab initio* frequencies. Thus while for any one configuration the map is not particularly accurate, for the ensemble as a whole it works surprisingly well.

B. Fluctuating transition dipoles

The projection of the transition dipole moment for the ith OH stretch on the laboratory-fixed p axis is approximately given by[23,40–42]

$$m_{ip}=\mu_i' x_i \hat{u}_i\cdot\hat{p}, \tag{12}$$

where μ_i' is the magnitude of the dipole derivative, x_i is the 0-1 matrix element of the OH stretch coordinate x ($x=r-r_0$, where r is the OH distance and r_0 is the equilibrium bond length), and $\hat{u}_i$ is the unit vector of the OH bond. The matrix element is easily calculated within the DVR scheme, and since the ground and excited local-mode vibrational states depend on the solvation environment, so does this matrix element. A simple way to parametrize this dependence is through the local-mode frequency; in Fig. 2, one sees that there is an outstanding linear correlation between the matrix element and the frequency. The linear fit is given in Table I and has a correlation coefficient of 1. The magnitude of the dipole derivative is given by $\mu'=|(d\vec{\mu}/dx)_{x=0}|$. To calculate this we begin by optimizing the OH bond length (using *ab initio* calculations) keeping the center of mass fixed. Then at this optimized structure a harmonic frequency calculation provides the dipole derivative. In Fig. 1, we also plot the ratio of the dipole derivative to that of the gas-phase versus the projection of the electric field along the OH bond. The dipole derivative is fitted well to a line with correlation coefficient 0.92 and rms deviation of 0.41; the formula for this line is given in Table I.

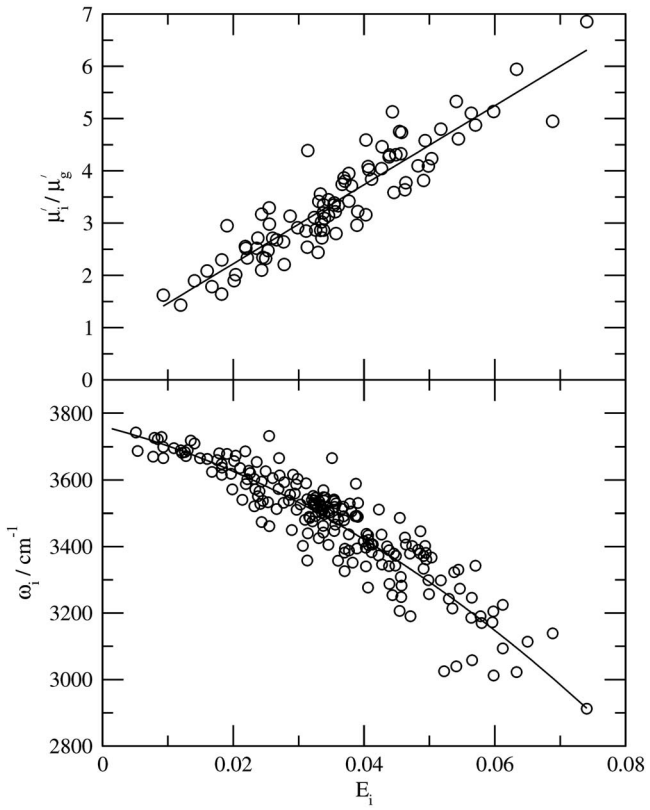

FIG. 1. Bottom panel: OH stretch frequencies, ω_i, for water clusters and the surrounding point charges vs electric field E_i (in a.u.). The solid line is the best quadratic fit (the formula for the fit is given in Table I). Top panel: Dipole derivative, μ_i', (relative to the gas-phase value) for water clusters and the surrounding point charges vs electric field E_i. The solid line is the best linear fit.

C. Fluctuating transition polarizabilities

To compute Raman spectra we need the transition polarizability for each local-mode OH stretch. In previous work it has been found that the isotropic transition polarizability is much less sensitive to solvation environment than is the transition dipole.[40,71] Therefore, in this work the effects of the varying transition polarizability will be ignored. In order to calculate the VV and VH spectra, however, we need to be able to determine the transition polarizability in the laboratory frame. A bond-polarizability model will be employed in this work, following that of others,[15,51] in which it is assumed that the transition polarizability has three constant components in the molecular frame, one along the bond and two identical components perpendicular to the bond. In ice it is believed that the ratio of the parallel and perpendicular

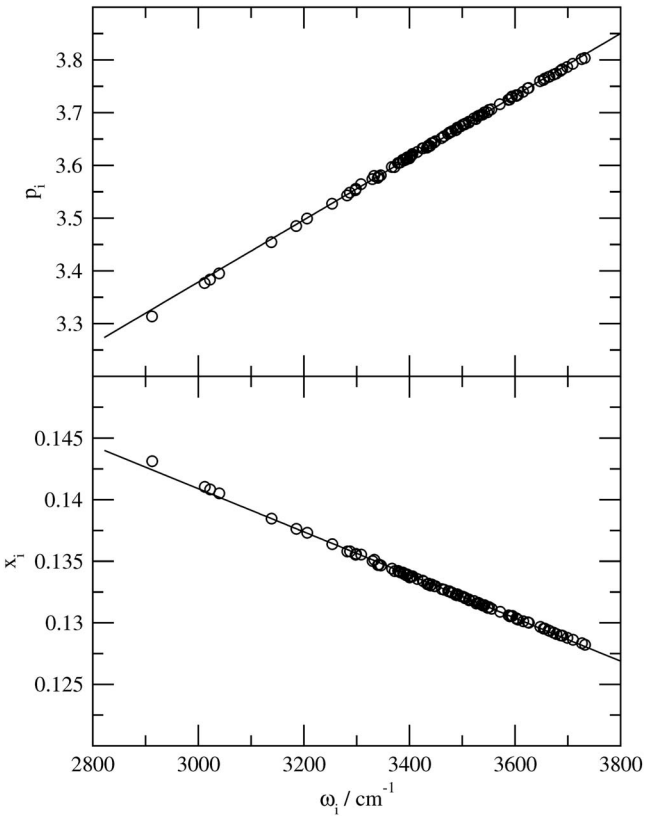

FIG. 2. Bottom panel: Position matrix elements, x_i (in a.u.), for water clusters and the surrounding point charges vs frequency ω_i. The solid line is the best linear fit. Top panel: Momentum matrix elements, p_i (in a.u.), for water clusters and the surrounding point charges vs frequency ω_i. The solid line is the best linear fit.

components of the transition polarizability is about 5.6,[72,73] and that value will be used in this study. Thus, for example,[15]

$$a_{iZZ} = \alpha'_{\perp} + (\alpha'_{\parallel} - \alpha'_{\perp})\cos^2\theta, \tag{13}$$

and

$$a_{iXY} = (\alpha'_{\parallel} - \alpha'_{\perp})\sin^2\theta\cos\phi\sin\phi, \tag{14}$$

where $\alpha'_{\parallel}$ and $\alpha'_{\perp}$ are the parallel and perpendicular bond-polarizability derivatives, and θ and ϕ are the usual polar and azimuthal angles of the OH bond vector in the laboratory frame.

D. Fluctuating intramolecular coupling

In the local-mode basis to lowest order the coupling frequency ω_{ij} between the two OH stretches on the same molecule is[74]

$$\hbar\omega_{ij} = k^a_{ij}x_i x_j + \cos(\phi)p_i p_j/m_{\mathrm{O}}, \tag{15}$$

where k^a_{ij} is the second derivative of the potential energy with respect to both bond lengths, evaluated at the minimum, x_i is the same position matrix element as before, p_i is the 0-1 momentum matrix element, ϕ is the HOH bond angle (tetrahedral in the case of SPC/E water), and m_{O} is the oxygen mass. The momentum matrix element can easily be calculated again within the DVR scheme.

For molecules in the liquid, each with its own solvation environment, the values of k^a_{ij}, x_i, and p_i are all different. x_i is parametrized with the local-mode frequency, as discussed above and shown in Table I. The momentum matrix element can also be fitted to the local-mode frequency, as shown in Fig. 2; the corresponding formula is given in Table I. To obtain the intramolecular coupling constants k^a_{ij}, a new set of 100 clusters was generated. These clusters, which are oxygen centered instead of hydrogen centered, were generated by choosing an oxygen at random in the simulation and including in the cluster any water with an oxygen within 4.07 Å of the central oxygen. The distance was chosen to give approximately the same number of waters in these clusters as in the hydrogen-centered clusters. Once again point charges were included up to a cutoff of 7.831 Å. The two bonds of the central water were again minimized keeping the center of mass fixed. A harmonic frequency calculation was performed at this minimum geometry to obtain the second derivative. Our strategy is once again to relate k^a_{ij} to the electric field on the hydrogen of the molecule of interest. We find that in this case k^a_{ij} is well correlated to the sum of the two electric field projections. In Fig. 3, we plot the *ab initio* k^a_{ij} versus E_i+E_j. There is a good linear correlation and the resulting fit is given in Table I. This leads to the formula for ω_{ij}:

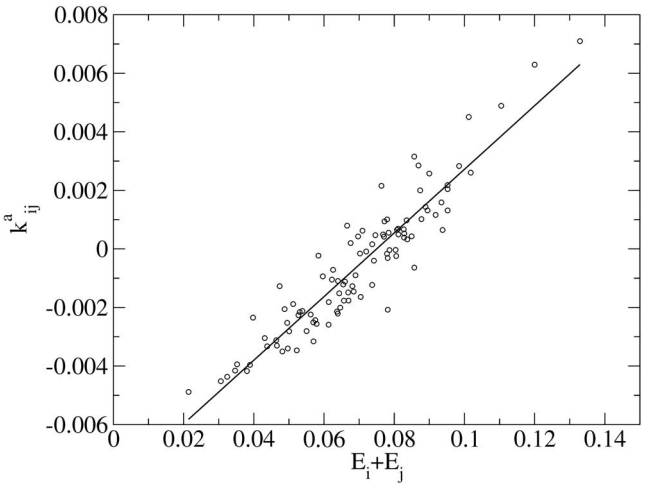

FIG. 3. Intramolecular coupling, k^a_{ij} (in a.u.), for water clusters and the surrounding point charges vs the electric field sum E_i+E_j (in a.u.). The solid line is the best linear fit.

$$\omega_{ij} = [\{-1789 + 23\,852(E_i + E_j)\}x_i x_j - 1.966 p_i p_j]\mathrm{cm}^{-1}, \tag{16}$$

and the formulas for the matrix elements in terms of the frequencies are given in Table I. When $E_i=E_j=0$, and x_i and p_i are evaluated for the gas-phase molecule ($\omega_i = 3707\ \mathrm{cm}^{-1}$), this gives $\omega_{ij} \simeq -58\ \mathrm{cm}^{-1}$, which is close to the value of about $-50\ \mathrm{cm}^{-1}$, as inferred from the gas-phase splitting between symmetric and antisymmetric stretch vibrations. Sampling molecules at random from a SPC/E MD simulation, and using the electric fields on the two hydrogens of each molecule to determine the local-mode frequencies, and then the relevant matrix elements, and finally the intramolecular coupling frequency, produces the distribution of these frequencies shown in Fig. 4. One sees that the average frequency, $-27.1\ \mathrm{cm}^{-1}$, is roughly half as small as in the gas phase, and that the distribution is quite wide.

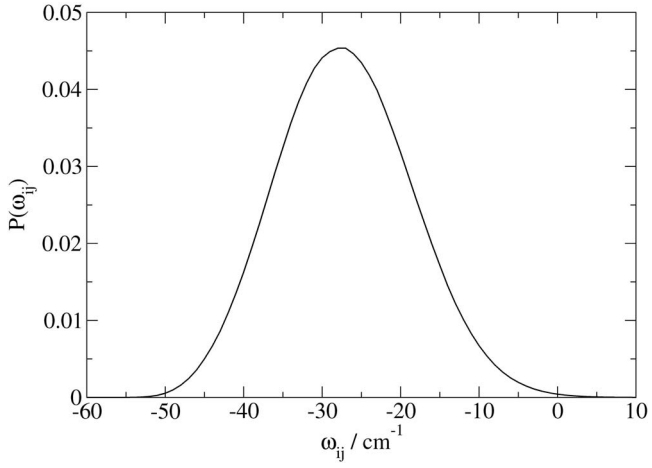

FIG. 4. Distribution of intramolecular coupling frequencies ω_{ij}.

E. Fluctuating intermolecular coupling

For the vibrational coupling between OH stretch chromophores on different molecules the simplest assumption is that of transition dipole interactions.[51,53] In this case the coupling frequency is given by

$$\hbar\omega_{ij} = k_{ij}^{e} x_i x_j, \tag{17}$$

where x_i is the same matrix element as before and k_{ij}^{e} is given by

$$k_{ij}^{e} = \mu_i' \mu_j' \{\hat{u}_i \cdot \hat{u}_j - 3[(\hat{u}_i \cdot \hat{n}_{ij})(\hat{u}_j \cdot \hat{n}_{ij})]\}/r_{ij}^{3}, \tag{18}$$

where $\hat{n}_{ij}$ is a unit vector along the line connecting the dipoles, and r_{ij} is the distance between the dipoles. A question arises: Where along each OH bond should one place the transition dipole? A number of different positions have been suggested;[53,75] here we turn to comparison with *ab initio* calculations to guide us. We will focus on a dimer within a cluster to determine where to place the dipole. This is a reasonable approach since one would expect the nearest-neighbor couplings to be the largest and most important ones. A set of 100 of the hydrogen-centered clusters was chosen. Then the closest oxygen to the hydrogen of interest in the cluster was determined. The four OH bonds in the resulting dimer were optimized and a harmonic frequency calculation was performed to determine the *ab initio* couplings for the four pairs of bonds. Then using the *ab initio* transition dipoles it was determined which spot along the bond gave the best fit between the *ab initio* coupling and the transition dipole coupling. We find that a position along the bond 0.58 Å from the oxygen gives the best fit. To assess the overall accuracy of the transition dipole approximation, in Fig. 5, we plot the *ab initio* coupling versus the transition dipole approximation to it. Despite significant scatter this is probably an acceptable approximation.

Using this transition dipole approximation and a SPC/E simulation, for a given OH chromophore one can calculate its largest (in magnitude) intermolecular coupling frequency. The average over many chromophores of these largest frequencies is -28 cm^{-1}, which can be compared to the average intramolecular coupling frequency of -27.1 cm^{-1}. Thus the magnitudes of the intramolecular and important intermolecular coupling frequencies are comparable (although for a given chromophore there are more of the latter than the former).

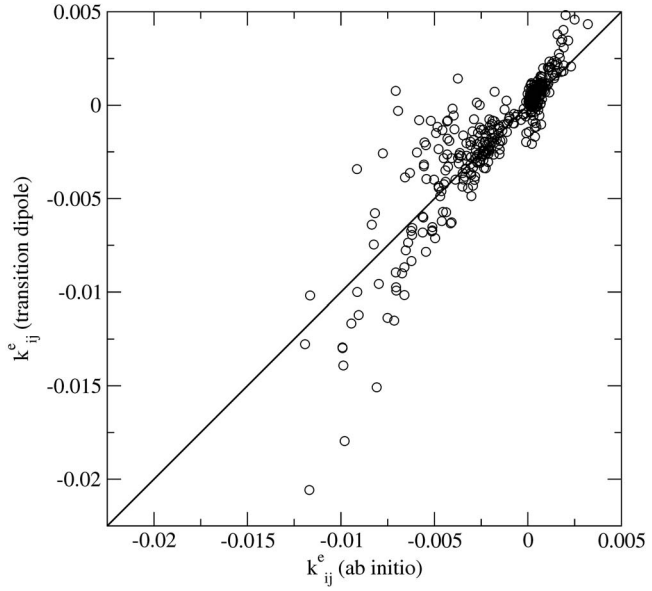

FIG. 5. Calculated (*ab initio*) intermolecular coupling k_{ij}^{e} (in a.u.) for water clusters surrounded by point charges vs transition dipole approximation obtained from Eq. (18).

IV. RESULTS

A. Molecular dynamics simulations

MD simulations of H_2O were performed using the SPC/E model.[67] Our *NVE* simulation contained 128 molecules at the experimental density at 298 K. Periodic boundary conditions were employed, and the electrostatic forces were computed using an approximation to the Ewald sum.[76] The classical equations of motion were integrated with the leapfrog algorithm with a 1 fs time step,[77] and the rotations were treated using quaternions.[78] Velocities were rescaled and equilibrated repeatedly until the desired temperature of 298 K was obtained.

At each step in the simulation, at each H atom the electric field from point charges on waters within the cutoff is computed. From this one obtains the local-mode frequencies ω_i. From the frequencies one obtains the matrix elements x_i and p_i, which together with the electric fields and the atomic positions allows one to obtain the intramolecular and intermolecular coupling frequencies ω_{ij}. Performing this for each time step produces the trajectory of the matrix $\kappa(t)$. Similarly, at each time step we calculate the dipole derviative μ_i', and from the instantaneous configurations one obtains $\hat{u}_i \cdot \hat{p}$, which allows one to calculate the dipole moment trajectory $m_{ip}(t)$. Using the bond-polarizability model, one obtains the trajectory $a_{ipq}(t)$. Thus from the simulation, one obtains the trajectories needed to calculate the spectra. Within the TAA, one needs to time average $\kappa(t)$ for a time T [as per Eq. (8)], diagonalize this average matrix, from each eigenvector compute the quantities $d_k(0)$ and $d_k(T)$ [see Eq. (10)], sum over all k, and then perform the ensemble average. The latter is

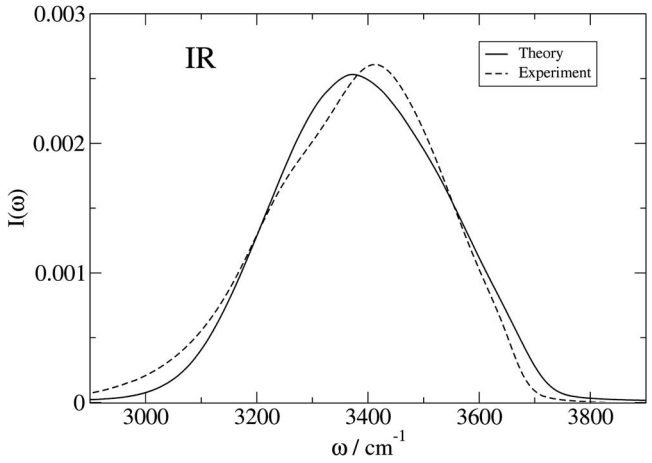

FIG. 6. Theoretical and experimental (Ref. 3) IR line shapes.

effected by time averaging $\kappa(t)$ over different pieces of the trajectory. The experimental lifetime, for use in $L(\omega)$, is $T_1 = 260$ fs.[79]

B. Line shape calculations

In order to calculate the IR and Raman line shapes within the TAA, we need to specify the averaging time T. To determine this time we follow our earlier suggestion,[55] calculating the line shape for the uncoupled chromophore, neglecting rotations, non-Condon effects, and lifetime broadening. Thus we use Eq. (3) to calculate the line shape, setting all couplings to zero, and setting the transition moments to 1 and the lifetime to infinity. For completeness we note that in these limits Eq. (3) reduces to the familiar form

$$I(\omega) \sim \mathrm{Re} \int_0^\infty dt e^{-i\omega t} \sum_i \left\langle \exp i \int_0^t d\tau \omega_i(\tau) \right\rangle. \tag{19}$$

The resulting line shape has a FWHM of $\Gamma = 349$ cm^{-1}. As previously discussed,[55] the averaging time is determined using the simple relationship $T = 5/\Gamma$. This results in an averaging time of $T = 76$ fs, which gave an excellent approximation to the motionally narrowered line shape,[55] and which will be used in all subsequent calculations.

We first focus on the IR line shape. In Fig. 6, we plot the calculated (298 K) and experimental[3] (298 K) line shapes, area normalized to the same value. The calculations agree well with the experiment, both in terms of position and FWHM, although the theory misses the weak shoulder at about 3250 cm^{-1}. Turning now to the Raman line shapes, the VV and VH line shapes are calculated using Eqs. (6) and (7), respectively. The normalized calculated (298 K) and the experimental[6] (295 K) VV and VH line shapes are plotted in Fig. 7. The theoretical VV line shape captures the double-peaked nature of the experiment, although the relative intensity of the two peaks is not quite right. Moreover the theory captures (but overemphasizes) the weak shoulder at 3650 cm^{-1}. The theoretical VH line shape is in good agreement with experiment, both in terms of its peak position and markedly asymmetric shape.

As discussed in the Introduction, both Buch *et al.*[51,52] and Torii[53] have recently performed similar spectral calculations for liquid water. Their calculations and ours involve many details, concerning frequency and coupling maps and calculations of spectroscopic observables, which differ among our three studies. For example, Torii does not include intramolecular coupling, and treated non-Condon effects with an adjustable parameter. Buch treated the ratio of the parallel and perpendicular bond-polarizability derivatives as an adjustable parameter, and used a somewhat different map for local-mode frequency fluctuations. In terms of the line shape calculations, Torii treated the coupled chromophore problem exactly by numerical integration of the Schrödinger equation, while Buch dealt with motional narrowing approximately by averaging the local-mode frequencies over 1 ps. Regarding line shape results, Torii's calculations for the isotropic and parallel-polarized Raman spectra and IR spectra are in qualitative agreement with experiment, although the splitting between the two peaks in the isotropic Raman spectrum is somewhat too large (compared to experiment). His calculations show that it is important to include non-Condon effects. Buch is primarily concerned with the vibrational sum-frequency-generation spectrum of the liquid-vapor interface, but does also present Raman (parallel- and perpendicular-polarized) and IR results for the bulk liquid (actually for the first five layers of a water slab) that are quite similar to ours.

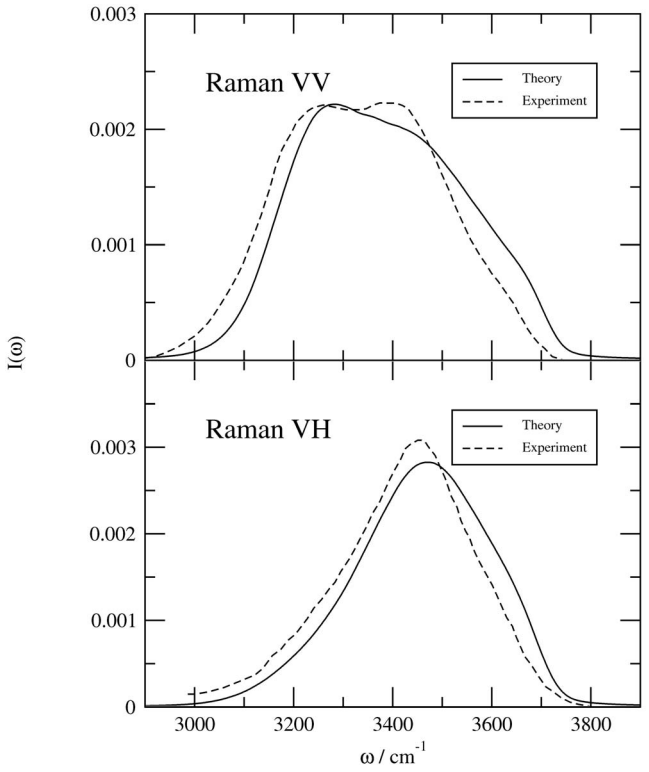

FIG. 7. Bottom panel: Theoretical and experimental (Ref. 6) Raman VH line shapes. Top panel: Theoretical and experimental (Ref. 6) Raman VV line shapes.

C. Line shape interpretations

Given that the theoretical line shapes provide a reasonable approximation to experiment, we can now attempt to understand the differences between the different line shapes,

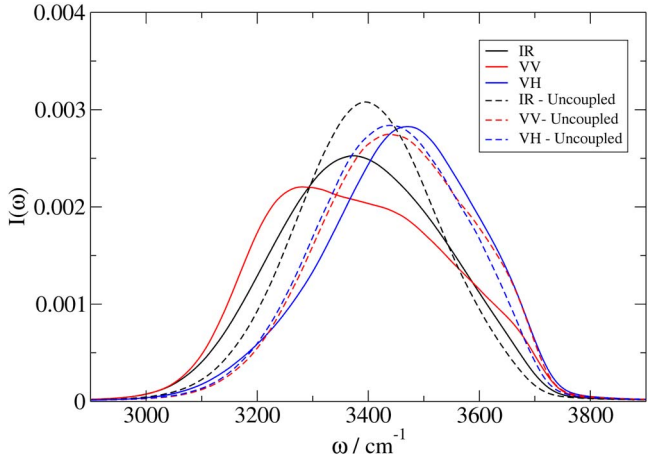

FIG. 8. (Color online) Theoretical IR and Raman VV and VH line shapes, and the same three line shapes when all coupling between chromophores is neglected.

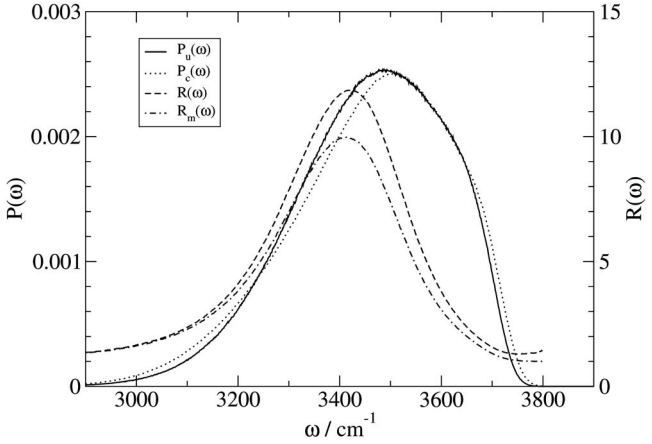

FIG. 9. Theoretical distributions of instantaneous frequencies for the uncoupled $[P_u(\omega)]$ and coupled $[P_c(\omega)]$ chromophores, and the inverse participation ratios $R(\omega)$ and $R_m(\omega)$.

and to interpret the various spectral features. As a first step in this direction, in Fig. 8 we show the theoretical IR and Raman VV and VH line shapes, all on the same graph, so one can see how different they really are. The three line shapes peak at about 3375, 3250, and 3475 cm^{-1}, respectively, and have distinctly different shapes. It is also instructive to calculate these same three line shapes but now in the absence of any coupling among chromophores; these results are also shown in the figure. One sees that for the VH line shape this makes a relatively small change, for the IR line shape the change is more pronounced, and for the VV line shape the change is quite dramatic indeed. We have also calculated these line shapes including only intramolecular coupling, and the results (not shown) are significantly closer to the uncoupled line shapes than to the fully coupled ones. These observations provide strong evidence that the origin of the somewhat mysterious peak at 3250 cm^{-1} in the VV Raman spectrum is due to the intermolecular coupling. Also note that our calculations for the uncoupled problem should yield reasonable approximations to the experimental line shapes for the OH stretch of dilute HOD in D_2O, which they do[23] (although here one should remark that the lifetime in the latter system is somewhat longer,[80] and the molecular dynamics is somewhat slower, both of which will have minor effects on the line shapes).

To examine this issue of coupling between OH stretch chomophores further, in Fig. 9 we compare the distribution of frequencies of the uncoupled chromophores to that for the fully coupled system. Thus the former is simply the distribution of local-mode frequencies ω_i, formally given by

$$P_u(\omega) = \langle \delta(\omega - \omega_i) \rangle. \tag{20}$$

This distribution shows a maximum at about 3490 cm^{-1}, and a shoulder that has been attributed to non-hydrogen-bonded OH chromophores[22,21,33,40] at about 3650 cm^{-1}. To obtain the distribution for the coupled system, at every time step we diagonalize $\kappa(t)$, and then the distribution is

$$P_c(\omega) = \frac{1}{2N} \sum_k \langle \delta(\omega - \omega_k) \rangle, \tag{21}$$

where ω_k are the $2N$ eigenvalues (N=128, the number of molecules). As shown in the figure, these two distributions are quite similar. Perhaps this is not too surprising, since the typical coupling matrix elements (−25 cm^{-1}) are quite a bit smaller in magnitude than the fluctuations in the diagonal frequencies [say, the FWHM, roughly 400 cm^{-1}, of $P_u(\omega)$].

Next we can consider the instantaneous eigenstates themselves. At each time step the κ matrix is diagonalized by the orthogonal transformation $B^T \kappa B$. One can get a rough idea about over how many local-mode chromophores the eigenstates extend by considering the inverse participation ratio:

$$R_k = \left(\sum_{i=1}^{2N} |B_{ik}|^4 \right)^{-1}. \tag{22}$$

For example, if eigenstate k is equally spread among n chromophores, then for n terms in the sum $|B_{ik}| = 1/\sqrt{n}$, and is zero for the other terms, and so $R_k = n$. Thus the value of the inverse participation ratio is roughly the number of chromophores involved in any given eigenstate. One can average R_k over eigenstates within a narrow frequency window to obtain $R(\omega)$, formally given by

$$R(\omega) = \frac{1}{2N} \sum_k \langle R_k \delta(\omega - \omega_k) \rangle / P_c(\omega). \tag{23}$$

This is also shown in Fig. 9. Remarkably, $R(\omega)$ is as large as 12 near the center of the band. Moreover even 100 cm^{-1} on either side it is still about 8. Thus the eigenstates are surprisingly delocalized. However, one can recall from studies of Anderson localization[81] that to produce localization (in the exponential sense) the width of the diagonal disorder must be significantly larger than that of the off-diagonal interactions, and even when the states are localized they can still extend over many chromophores. Thus in terms of delocalization, a little coupling goes a long way!

It is also of interest to determine, on the average, if the eigenstates extend primarily over OH groups on different

molecules, or over both OH groups on each involved molecule. That is, if an eigenstate extends over n OH chromophores, are these chromophores on as many as n molecules, or are they on closer to $n/2$ molecules? To this end, let us replace the chromophore label i by an equivalent set of two indices: α, which runs over the N molecules, and β, which goes from 1 to 2, indicating the two OH chromophores on each molecule. We can then define a *molecular* inverse participation ratio for each eigenstate k, by

$$R_{mk} = \left(\sum_{\alpha=1}^{N} \left\{ \sum_{\beta=1}^{2} |B_{\alpha\beta k}|^2 \right\}^2 \right)^{-1}. \tag{24}$$

Consider again the situation where an eigenstate is equally spread over n chromophores, such that for n $\alpha\beta$ pairs $|B_{\alpha\beta k}| = 1/\sqrt{n}$ (while the others are zero). If the eigenstate involves OH groups on different molecules, then for each involved molecule only one term (with $\beta=1$ *or* 2) contributes, and so $R_{mk}=n$. On the other hand, if the eigenstate is on both OH groups of each involved molecule, then for those molecules terms with $\beta=1$ and 2 both contribute, leading to $R_{mk}=n/2$. Thus in either case R_{mk} is roughly the number of molecules over which the eigenstate extends. One can average over eigenstates as in Eq. (23) to obtain $R_m(\omega)$. This is also shown in Fig. 9. One sees that $R_m(\omega)$ is closer to $R(\omega)$ than to $R(\omega)/2$, showing that for the most part the eigenstates extend over OH groups on different molecules. Thus, for example, at the center of the band, the eigenstates extend over approximately ten molecules. Similar conclusions were reached by Buch *et al.* in their analysis of the eigenstates in the top five layers of water at the liquid-vapor interface.[52]

In order to understand the effects of delocalization on spectroscopy, it is instructive to consider the line shapes in the inhomogeneous limit (that is, when dynamical effects are neglected). For this exercise we will also neglect lifetime broadening. In this limit $\kappa(t)$ can be replaced by its initial value in Eq. (4), and so $F(t)=e^{i\kappa(0)t}$, in which case the IR line shape is given by[55]

$$I(\omega) \sim \sum_k \langle d_k^2 \delta(\omega - \omega_k) \rangle, \tag{25}$$

where

$$d_k = \sum_i m_{ip}(0) B_{ik}. \tag{26}$$

As before, for the Raman line shapes m_{ip} is replaced by a_{ipq}. Recall that B is the matrix that diagonalizes $\kappa(0)$. This inhomogeneous line shape can be written in normalized fashion as

$$P_w(\omega) = \sum_k \langle d_k^2 \delta(\omega - \omega_k) \rangle \Big/ \sum_k \langle d_k^2 \rangle, \tag{27}$$

for comparison with other normalized frequency distributions.

Thus in this limit the normalized line shape is a weighted frequency distribution, where the weighting factor is d_k^2. The IR and Raman VV and VH spectra differ because in each case d_k is a different linear combination of the expansion coefficients B_{ik}. m_{ip} and a_{ipq} involve different orientation factors, and in addition, m_{ip} involves non-Condon effects. Let us first ignore these differences, and let $m_{ip}=a_{ipq}=1$, in which case

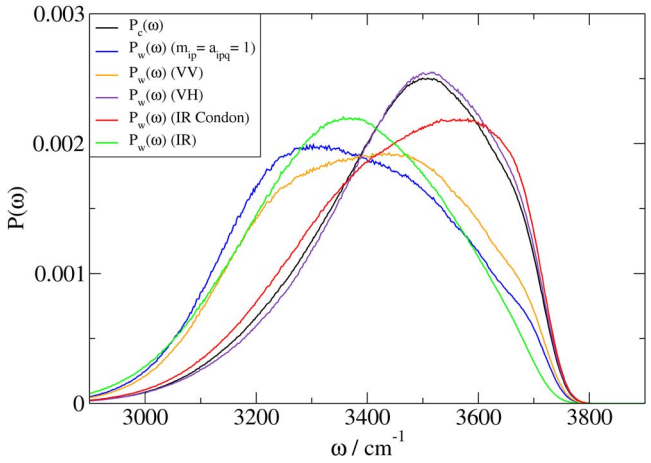

FIG. 10. (Color online) Theoretical distribution of instantaneous frequencies for the coupled chromophores, as well as weighted frequency distributions under the various circumstances described in the text.

$$d_k = \sum_i B_{ik} \tag{28}$$

simply involves linear combinations of the expansion coefficients alone. Under these conditions, we compare $P_w(\omega)$ to $P_c(\omega)$ in Fig. 10. Remarkably, $P_w(\omega)$ is very different from $P_c(\omega)$, peaking at about 3250 cm^{-1}, with shoulders at about 3475 and 3700 cm^{-1}, the latter two of which are near the characteristic frequencies of the (coupled) frequency distribution itself. Thus the seemingly modest coupling between the local modes, which indeed produces a modest change in the frequency distribution, produces a weighted frequency distribution (relevant for the spectroscopy) that is dramatically different from the frequency distribution itself, including the introduction of a new frequency at about 3250 cm^{-1}. In addition, it is clear that the latter is a direct result of the significant delocalization of the eigenstates. This intensity enhancement at low frequencies is reminiscent of, and indeed has the same origin as, the enhanced optical activity of the eigenstate at the bottom of the exciton band for linear arrays with negative coupling among local-mode states.[82] This discussion corroborates earlier arguments in favor of collective excitations in liquid water and their role in vibrational spectra.[10,11,15,16,52]

In Fig. 10 we also show the weighted distributions relevant for the Raman line shapes, that is, when the angular factors a_{ipq} in Eq. (26) are included. One sees that the distributions relevant for the VV and VH spectra are dramatically different. The VH distribution is very similar to the frequency distribution itself, while the VV distribution is similar to the weighted distribution (making the Condon approximation and neglecting rotations) described above. Presumably this is because a_{ipp} [see, for example, Eq. (13)] has a constant term, and so d_k is more similar to Eq. (28), whereas for a_{ipq} [see, for example, Eq. (14)] the different orientations of the different chromophores partially destroy the linear combination. In the same figure we also show the

relevant distribution for the IR spectrum, but within the Condon approximation (only including the rotational contribution), that is, taking $m_{ip}=\hat{u}_i\cdot\hat{p}$. This is somewhat different from both Raman distributions, but is more similar to the VH distribution. Finally, we show the relevant distribution for the IR spectrum, including non-Condon effects [that is, m_{ip} is given by Eq. (12)]. As expected,[40] we see that these non-Condon effects significantly shift the IR distribution to the red.

In summary, then, we see that the relatively modest coupling between local-mode chromophores produces a relatively small difference between the distributions of local-mode frequencies and of frequencies for the coupled chromophores. On the other hand, the coupling is large enough to delocalize the instantaneous eigenstates over up to 12 chromphores. In terms of spectroscopy, this delocalization has profound consequences, as it significantly affects the weighting of the different eigenstates. In particular, this delocalization is responsible for the appearance of a new collective characteristic frequency at about 3250 cm^{-1}. The IR and Raman VV and VH spectra are all different because of the different angular factors in the linear combinations in Eq. (26). Circumstances are such that in the VV spectrum the collective mode is prominent, whereas in the VH and IR spectra it is not. The IR spectrum is significantly redshifted from the VH spectrum due to the non-Condon effects.

V. CONCLUSION

The vibrational spectroscopy of neat liquids presents a formidable theoretical challenge because of the computational difficulty in dealing with coupling between chromophores (the vibrational exciton problem) and the effects of dynamics (motional narrowing). We have presented theoretical calculations of the Raman and IR line shapes for water in the OH stretching region. We have extended our ES/MD method[33] to calculate trajectories of not only the OH stretching frequencies and transition dipoles and polarizabilities but also the couplings between vibrational modes. We find that intramolecular coupling is non-negligible and varies considerably from molecule to molecule (as a result of different molecular environments). The intermolecular couplings are more difficult to approximate—we used the familiar transition dipole model. To account for dynamical effects, we used a recently developed time-averaging approximation.[55] The experimental IR and Raman VV and VH spectra are quite different from each other. Our theoretical results are in good agreement with experiment and reasonably accurately capture these differences.

The interpretation of these experimental spectra and their differences has been controversial. Our analysis indicates that even though the coupling between OH stretch chromophores is relatively modest, the instantaneous vibrational eigenstates are delocalized over a substantial (up to 12) number of chromophores. This delocalization has a profound impact on the spectroscopy, producing a collective mode centered at around 3250 cm^{-1}. The other characteristic frequencies appear as the peak in the local-mode distribution of frequencies at about 3490 cm^{-1}, and the shoulder in the same distribution at about 3650 cm^{-1} due to hydrogen atoms not involved in hydrogen bonds. The experimental IR and Raman VV and VH spectra emphasize these three characteristic frequencies to different extents. In particular, the VV spectra shows a pronounced peak at about 3250 cm^{-1} due to this collective mode. The IR spectrum is redshifted from the local-mode peak at 3490 cm^{-1} as a result of non-Condon effects. Our analysis, which emphasizes the role of coupling between chromophores, indicates that for neat liquid H_2O spectral peaks cannot be meaningfully assigned to individual molecules in different molecular environments. Moreover, substantial symmetry breaking due to the local molecular environment means that the symmetric and antisymmetric normal modes of water are not a useful basis, and it is not meaningful to make spectral feature assignments based on these normal modes.

Despite these successes there remains room for improvement in the theoretical calculations. There surely exist better maps from nuclear coordinates of the liquid molecules to the OH stretch frequency of a tagged bond, as well as better maps for the transition dipoles and polarizabilities and the intramolecular coupling. One can surely improve upon the transition dipole approximation for the intermolecular coupling.[83] One should probably include the bend vibrational degrees of freedom, as they may couple to the stretches through a 2:1 Fermi resonance. As mentioned earlier, using a classical simulation model, especially with regard to the librations, may be problematic.

One exciting prospect of this work is that it can easily be extended to other important situations such as the Raman and IR spectra of ice *Ih*, and the vibrational sum-frequency-generation spectroscopy of the water liquid-vapor interface. Interpretations of these spectra have also been controversial, and we hope that our theory and results for these systems (which we intend to report on shortly) will be accurate enough to help resolve these issues. In addition, the TAA can be extended to nonlinear ultrafast spectroscopy,[84] meaning that one is now in the position of calculating two-dimensional IR spectra for liquid water, which would allow for direct comparison to results from exciting new experiments.[85,86]

ACKNOWLEDGMENTS

We are grateful for support from the National Science Foundation, through Grant Nos. CHE-0446666 and CHE-0750307. We thank Professor Will Polik and Hope College for the use of their MU3C computer cluster, on which some of the calculations reported herein were performed. We thank Steve Corcelli for helpful conversations during the early stages of this work.

[1] J. E. Bertie, M. K. Ahmed, and H. H. Eysel, J. Phys. Chem. **93**, 2210 (1989).
[2] J. B. Brubach, A. Mermet, A. Filabozzi, A. Gerschel, and R. Roy, J. Chem. Phys. **122**, 184509 (2005).
[3] J. E. Bertie and Z. Lan, Appl. Spectrosc. **50**, 1047 (1996).
[4] W. F. Murphy and H. J. Bernstein, J. Phys. Chem. **76**, 1147 (1972).
[5] J. R. Scherer, M. K. Go, and S. Kint, J. Phys. Chem. **78**, 1304 (1974).
[6] G. E. Walrafen, M. R. Fischer, M. S. Hokmabadi, and W. H. Yang, J. Chem. Phys. **85**, 6970 (1986).

[7] D. M. Carey and G. M. Korenowski, J. Chem. Phys. **108**, 2669 (1998).
[8] G. E. Walrafen, J. Chem. Phys. **47**, 114 (1967).
[9] G. D'Arrigo, G. Maisano, F. Mallamace, P. Migliardo, and F. Wanderlingh, J. Chem. Phys. **75**, 4264 (1981).
[10] J. L. Green, A. R. Lacey, and M. G. Sceats, J. Phys. Chem. **90**, 3958 (1986).
[11] D. E. Hare and C. M. Sorensen, J. Chem. Phys. **96**, 13 (1992).
[12] D. A. Schmidt and K. Miki, J. Phys. Chem. A **111**, 10119 (2007).
[13] P. L. Geissler, J. Am. Chem. Soc. **127**, 14930 (2005).
[14] M. Falk and T. A. Ford, Can. J. Chem. **44**, 1699 (1966).
[15] A. Belch and S. Rice, J. Chem. Phys. **78**, 4817 (1983).
[16] S. Rice, M. Bergren, A. Belch, and N. Nielson, J. Phys. Chem. **87**, 4295 (1983).
[17] T. T. Wall and D. F. Hornig, J. Chem. Phys. **43**, 2079 (1965).
[18] G. E. Walrafen, J. Chem. Phys. **48**, 244 (1968).
[19] J. D. Smith, C. D. Cappa, K. R. Wilson, R. C. Cohen, P. L. Geissler, and R. J. Saykally, Proc. Natl. Acad. Sci. U.S.A. **102**, 14171 (2005).
[20] R. Kumar, J. R. Schmidt, and J. L. Skinner, J. Chem. Phys. **126**, 204107 (2007).
[21] C. P. Lawrence and J. L. Skinner, J. Chem. Phys. **118**, 264 (2003).
[22] C. P. Lawrence and J. L. Skinner, Chem. Phys. Lett. **369**, 472 (2003).
[23] B. Auer, R. Kumar, J. R. Schmidt, and J. L. Skinner, Proc. Natl. Acad. Sci. U.S.A. **104**, 14215 (2007).
[24] D. W. Oxtoby, D. Levesque, and J.-J. Weis, J. Chem. Phys. **68**, 5528 (1978).
[25] D. W. Oxtoby, Adv. Chem. Phys. **47**, 487 (1981).
[26] C. P. Lawrence and J. L. Skinner, J. Chem. Phys. **117**, 8847 (2002).
[27] L. Ojamäe, K. Hermansson, and M. Probst, Chem. Phys. Lett. **191**, 500 (1992).
[28] R. Rey, K. B. Møller, and J. T. Hynes, J. Phys. Chem. A **106**, 11993 (2002).
[29] K. B. Møller, R. Rey, and J. T. Hynes, J. Phys. Chem. A **108**, 1275 (2004).
[30] J. D. Eaves, A. Tokmakoff, and P. L. Geissler, J. Phys. Chem. A **109**, 9424 (2005).
[31] E. Harder, J. D. Eaves, A. Tokmakoff, and B. J. Berne, Proc. Natl. Acad. Sci. U.S.A. **102**, 11611 (2005).
[32] K. Hermansson, S. Knuts, and J. Lindgren, J. Chem. Phys. **95**, 7486 (1991).
[33] S. A. Corcelli, C. P. Lawrence, and J. L. Skinner, J. Chem. Phys. **120**, 8107 (2004).
[34] J. R. Schmidt, S. A. Corcelli, and J. L. Skinner, J. Chem. Phys. **121**, 8887 (2004).
[35] T. Hayashi, T. l. C. Jansen, W. Zhuang, and S. Mukamel, J. Phys. Chem. A **109**, 64 (2005).
[36] T. l. C. Jansen, T. Hayashi, W. Zhuang, and S. Mukamel, J. Chem. Phys. **123**, 114504 (2005).
[37] R. Kubo, Adv. Chem. Phys. **15**, 101 (1969).
[38] L. Ojamäe, J. Tegenfeldt, J. Lindgren, and K. Hermansson, Chem. Phys. Lett. **195**, 97 (1992).
[39] D. W. Oxtoby, Adv. Chem. Phys. **40**, 1 (1979).
[40] S. A. Corcelli and J. L. Skinner, J. Phys. Chem. A **109**, 6154 (2005).
[41] J. R. Schmidt, S. A. Corcelli, and J. L. Skinner, J. Chem. Phys. **123**, 044513 (2005).
[42] J. R. Schmidt, S. T. Roberts, J. J. Loparo, A. Tokmakoff, M. D. Fayer, and J. L. Skinner, Chem. Phys. **341**, 143 (2007).
[43] P. Bouř, Chem. Phys. Lett. **365**, 82 (2002).
[44] J. R. Reimers and R. O. Watts, Chem. Phys. **91**, 201 (1984).
[45] J. Martí, J. A. Padró, and E. Guàrdia, J. Mol. Liq. **62**, 17 (1994).
[46] J. Martí, E. Guàrdia, and J. A. Padró, J. Chem. Phys. **101**, 1083 (1994).
[47] H. Ahlborn, X. Ji, B. Space, and P. B. Moore, J. Chem. Phys. **111**, 10622 (1999).
[48] H. Ahlborn, B. Space, and P. B. Moore, J. Chem. Phys. **112**, 8083 (2000).
[49] R. Bansil, T. Berger, K. Toukan, M. A. Ricci, and S. H. Chen, Chem. Phys. Lett. **132**, 165 (1986).
[50] P. L. Silvestrelli, M. Bernasconi, and M. Parrinello, Chem. Phys. Lett. **277**, 478 (1997).
[51] V. Buch, J. Phys. Chem. B **109**, 17771 (2005).
[52] V. Buch, T. Tarbuck, G. L. Richmond, H. Groenzin, I. Li, and M. J. Schultz, J. Chem. Phys. **127**, 204710 (2007).
[53] H. Torii, J. Phys. Chem. A **110**, 9469 (2006).
[54] V. Buch, S. Bauerecker, J. P. Devlin, U. Buck, and J. K. Kazimirski, Int. Rev. Phys. Chem. **23**, 375 (2004).
[55] B. Auer and J. L. Skinner, J. Chem. Phys. **127**, 104105 (2007).
[56] T. l. C. Jansen, W. Zhuang, and S. Mukamel, J. Chem. Phys. **121**, 10577 (2004).
[57] T. l. C. Jansen, A. G. Dijkstra, T. M. Watson, J. D. Hirst, and J. Knoester, J. Chem. Phys. **125**, 044312 (2006).
[58] T. l. C. Jansen and J. Knoester, J. Phys. Chem. B **110**, 22910 (2006).
[59] S. Mukamel and D. Abramavicius, Chem. Rev. (Washington, D.C.) **104**, 2073 (2004).
[60] W. Zhuang, D. Abramavicius, T. Hayashi, and S. Mukamel, J. Phys. Chem. B **110**, 3362 (2006).
[61] J. Choi, S. Hahn, and M. Cho, Int. J. Quantum Chem. **104**, 616 (2005).
[62] K. F. Everitt, C. P. Lawrence, and J. L. Skinner, J. Phys. Chem. B **108**, 10440 (2004).
[63] S. Hahn, S. Ham, and M. Cho, J. Phys. Chem. B **109**, 11789 (2005).
[64] J.-H. Choi, H. Lee, K.-K. Lee, S. Hahn, and M. Cho, J. Chem. Phys. **126**, 045102 (2007).
[65] R. D. Gorbunov, P. H. Nguyen, M. Kobus, and G. Stock, J. Chem. Phys. **126**, 054509 (2007).
[66] T. l. C. Jansen, D. Cringus, and M. S. Pshenichnikov (unpublished).
[67] H. J. C. Berendsen, J. R. Grigera, and T. P. Straatsma, J. Chem. Phys. **91**, 6269 (1987).
[68] D. A. McQuarrie, *Statistical Mechanics* (Harper & Row, New York, 1976).
[69] M. J. Frisch, G. W. Trucks, H. B. Schlegel, and G. E. Scuseria *et al.*, GAUSSIAN 03, Gaussian Inc., Pittsburgh PA, (2003).
[70] D. Colbert and W. H. Miller, J. Chem. Phys. **96**, 1982 (1992).
[71] A. Morita and J. T. Hynes, Chem. Phys. **258**, 371 (2000).
[72] J. G. Scherer and R. G. Snyder, J. Chem. Phys. **67**, 4794 (1977).
[73] J. E. Bertie, B. F. Francis, and J. R. Scherer, J. Chem. Phys. **73**, 6352 (1980).
[74] E. B. Wilson, J. C. Decius, and P. C. Cross, *Molecular Vibrations* (Dover, New York 1980).
[75] J. Sadlej, V. Buch, J. K. Kazimirski, and U. Buck, J. Phys. Chem. A **103**, 4933 (1999).
[76] D. J. Adams and G. S. Dubey, J. Comput. Phys. **72**, 156 (1987).
[77] M. P. Allen and D. J. Tildesley, *Computer Simulation of Liquids* (Clarendon, Oxford, 1987).
[78] M. Svanberg, Mol. Phys. **92**, 1085 (1997).
[79] A. J. Lock and H. J. Bakker, J. Chem. Phys. **117**, 1708 (2002).
[80] C. J. Fecko, J. J. Loparo, S. T. Roberts, and A. Tokmakoff, J. Chem. Phys. **122**, 054506 (2005).
[81] J. L. Skinner, J. Phys. Chem. **98**, 2503 (1994).
[82] D.-J. Heijs, A. G. Dijkstra, and J. Knoester, Chem. Phys. **341**, 230 (2007).
[83] P. Hamm and S. Woutersen, Bull. Chem. Soc. Jpn. **75**, 985 (2002).
[84] T. l. C. Jansen, and W. M. Ruszel (unpublished).
[85] M. L. Cowan, B. D. Bruner, N. Huse, J. R. Dwyer, B. Chugh, E. T. J. Nibbering, T. Elsaesser, and R. D. J. Miller, Nature (London) **434**, 199 (2005).
[86] D. Kraemer, M. L. Cowan, A. Paarmann, N. Huse, E. T. J. Nibbering, T. Elsaesser, and R. J. D. Miller, Proc. Natl. Acad. Sci. U.S.A. **105**, 437 (2008).